Nanotechnology **19** (2008) 035608 (7pp) doi:10.1088/0957-4484/19/03/035608

Morphological and structural modulation of $PbWO_4$ crystals directed by dextrans

Jinhu Yang, Conghua Lu, Hong Su, Jiming Ma, Humin Cheng and Limin Qi[1]

Beijing National Laboratory for Molecular Sciences (BNLMS), State Key Laboratory for Structural Chemistry of Stable and Unstable Species, College of Chemistry, Peking University, Beijing 100871, People's Republic of China

E-mail: liminqi@pku.edu.cn

Received 12 August 2007, in final form 23 October 2007
Published 11 December 2007
Online at stacks.iop.org/Nano/19/035608

Abstract

A facile, dextran-directed solution route for the morphology- and structure-controlled synthesis of $PbWO_4$ crystals, such as monoclinic raspite $PbWO_4$ nanobelts and tetragonal stolzite $PbWO_4$ crystals with penniform and wheat-ear-like morphologies, has been demonstrated. Three differently charged dextrans were employed for the $PbWO_4$ crystallization and they turned out to be very effective in the morphological and structural modulation of $PbWO_4$ crystals, as evidenced by the scanning electron microscopy (SEM), transmission electron microscopy (TEM), x-ray diffraction (XRD) and Raman spectroscopy characterizations. In particular, novel monoclinic raspite $PbWO_4$ nanobelts were produced under the direction of anionic dextran with a suitable concentration, probably due to the specific interactions between SO_4^{2-} groups from anionic dextran molecules and Pb^{2+} ions from $PbWO_4$ crystals. To the best of our knowledge, this is the first synthesis of monoclinic raspite $PbWO_4$ in the laboratory, which usually exists as a natural crystal. In addition, the photoluminescence properties of the obtained $PbWO_4$ crystals with different morphologies and crystal structures have been characterized and discussed, which provides useful information for the fundamental investigation and potential application of $PbWO_4$ crystals.

1. Introduction

The controlled synthesis of inorganic nano- and microcrystals with specific size, shape and structure is of fundamental significance in modern material science and engineering, because the size, shape and structure could determine not only the relevant optical, electronic and magnetic properties of the materials themselves but also the performances of those material-based devices for applications [1–5]. Since the discovery of carbon nanotubes, one-dimensional (1D) nanostructures such as nanorods, nanotubes and nanobelts have become a hotspot of considerable research due to their unique properties of optical excitation and electron transport and thereby promising potential for nanodevice fabrication [6–9]. In particular, inorganic nanobelts/nanoribbons, a relatively new group of 1D nanostructures with a rectangular cross section, are attracting considerable interest [8, 10, 11].

Recently, many efforts have been made to synthesize tungstate crystals with controlled morphologies because of their excellent luminescent properties and promising applications. For example, $CdWO_4$ rods [12, 13], $ZnWO_4$ rods/belts [14], $BaWO_4$ plates [15] and $MnWO_4$ fibres [16] were synthesized by the hydrothermal/solvothermal method while $BaWO_4$ rods/wires as well as their assemblies were obtained by reverse micelle-based synthesis [17–19]. As a member of the tungstate family, lead tungstate is a kind of important inorganic scintillating crystal. There are two different polymorphs of lead tungstate: one is commonly found stolzite with the tetragonal symmetry and the other one is rarely found raspite with the monoclinic symmetry, which transforms to stolzite irreversibly around 400 °C [20]. Stolzite $PbWO_4$ with a scheelite structure can be easily synthesized and its excellent properties, such as high density (8.2 g cm^{-3}), short decay time (less than 10 ns) and high resistance for radiation damage, etc, have been determined [21, 22]. Hence stolzite has been successfully used in laser and stimulated

[1] Author to whom any correspondence should be addressed.

Raman scattering, especially chosen as a promising scintillating medium for the electromagnetic (EM) colorimeter in the Large Hadron Collider (LHC) at CERN [23]. On the other hand, as a rare natural crystal, raspite $PbWO_4$ has not yet been successfully prepared in the laboratory and only limited optical and spectroscopic investigations have been made on natural raspite $PbWO_4$ crystal [20, 24, 25]. It is known that raspite has a unit cell volume very close to stolzite (difference less than 1%) and raspite crystals adopt some physical properties similar to stolzite crystals (e.g. high density and short decay time); however, the optical properties of $PbWO_4$ are very sensitive to its structure. Therefore, the development of synthetic routes to raspite $PbWO_4$ crystals is demanding for fully exploring the properties and potential applications of $PbWO_4$ crystals. In recent decades, considerable progress has been made on the controlled synthesis of $PbWO_4$ nano- and microcrystals by the traditional Czochralski [26] and Bridgeman [27] methods as well as newly developed wet chemical routes, such as polymer/surfactant-directed synthesis [28–35], microemulsions-mediated synthesis [29, 36, 37], sonochemical methods [38, 39] and microwave-assisted ways [40]. However, all the obtained $PbWO_4$ crystals up to date have the structure of tetragonal stolzite and it remains a great challenge to synthesize monoclinic raspite $PbWO_4$ crystals with controlled size and morphology.

Based on the understanding of biomineralization processes where biomacromolecules precisely control the nucleation, growth and patterning of inorganic minerals to form highly ordered architectures, many kinds of synthetic polymers and biomacromolecules have been employed for the biomimetic synthesis of inorganic materials with modulated morphologies and architectures [41–45]. Recently, we have demonstrated that the biomacromolecule dextran can be used as an effective crystal growth modifier for the morphology-controlled synthesis of Ag [46] and Ag_3PO_4 [47] crystals, which inspired us to explore the application of dextran in other material systems. Herein, we report a facile route to synthesize $PbWO_4$ crystals with modulated morphologies and structures, such as monoclinic raspite $PbWO_4$ nanobelts and tetragonal stolzite $PbWO_4$ crystals with penniform and wheat-ear-like morphologies, under the direction of three differently charged dextrans. To the best of our knowledge, this is the first synthesis of monoclinic raspite $PbWO_4$ in the laboratory.

2. Experimental section

2.1. Materials

The nonionic dextran (Dex-40, MW 40 000) and the anionic dextran, dextran sulfate (DexS-40, MW 40 000), were purchased from Roth (Germany) and the cationic dextran, aminated dextran (AM-Dex-5, MW 5000), was purchased from Aldrich Company, respectively. All the other chemical reagents were of analytical grade and the water used was deionized.

2.2. Synthesis of $PbWO_4$ crystals

Generally, a certain amount (e.g. 0.01 g) of dextrans (e.g. Dex-40, DexS-40 or AM-Dex-5), 0.5 ml of 0.1 M Na_2WO_4 solution and 9 ml water were mixed first. After the dextrans were dissolved completely and the solution was thermostatted at 20 °C, 0.5 ml of 0.1 M $Pb(NO_3)_2$ solution was added under vigorous stirring, resulting in a white precipitation. After the reaction solution was kept for 1 day, the products were collected and characterized.

2.3. Characterization

Scanning electron microscopy (SEM) measurements were performed with an Amray 1910FE microscope operated at 10 kV. Transmission electron microscopy (TEM) and high-resolution TEM (HRTEM) observations were conducted on a JEOL JEM-200CX microscope operated at 160 kV and a Hitachi H-9000HAR microscope at 300 kV, respectively. Powder x-ray diffraction (XRD) patterns were recorded on a Rigaku Dmax-2000 diffractometer with Cu Kα radiation. Raman spectra were measured on a Renishaw 1000 Raman spectrometer with He–Ne power source at 633 nm and photoluminescence (PL) spectra were recorded on a Hitachi F-4500 spectrofluorometer at room temperature.

3. Results and discussion

3.1. Characterization of monoclinic raspite $PbWO_4$ nanobelts

$PbWO_4$ nanobelts were readily synthesized in the presence of DexS-40 at a concentration of 1 g l^{-1} (figure 1). As shown in the overview picture (figure 1(a)), the product is apparently uniform and rod-like with lengths as long as 10 μm. From the enlarged pictures (figures 1(b) and (c)), it is observed that some ribbons were folded or circumnutated, indicating that the product was actually nanoribbons. The width of these nanoribbons mostly ranged from 100 to 150 nm, corresponding to a high aspect ratio of about 50–100. Judging from the side faces, the average thickness of the nanoribbons is about 10 nm (figure 1(c)). The XRD pattern (figure 1(d)) of the nanoribbons shows sharp reflections corresponding to a monoclinic raspite structure of $PbWO_4$ crystals (JCPDS card no. 13-026) and the diffraction peaks of (200) and (400) are overwhelmingly intensive, indicating that the top faces of the nanoribbons are the (200) planes. In addition, the corresponding Raman spectrum (figure 1(e)) shows peaks at 182, 282, 300, 395, 494, 523, 644, 670, 747 and 870 cm^{-1}, characteristic of raspite $PbWO_4$ crystals [25], confirming that the nanobelts were actually $PbWO_4$ crystals of the raspite structure. However, the two weak peaks at 117 and 142 cm^{-1} have not been observed from natural raspite $PbWO_4$ crystals [25], which is worthy of further investigation. To the best of our knowledge, this is the first time for the synthesis of monoclinic $PbWO_4$ crystals of the raspite structure in the laboratory.

Figure 2 shows the typical TEM and HRTEM images of an individual nanoribbon as well as its electron diffraction (ED) pattern. The TEM image of a single nanoribbon shown in figure 2(a) displays a uniform width of 120 nm, which is consistent with the SEM observation above. The ED pattern of a single nanoribbon exhibits a set of sharp spots with spacing of 4.98, 5.30 and 3.62 Å, corresponding to the {010}, {001} and {011} reflections, respectively. This result

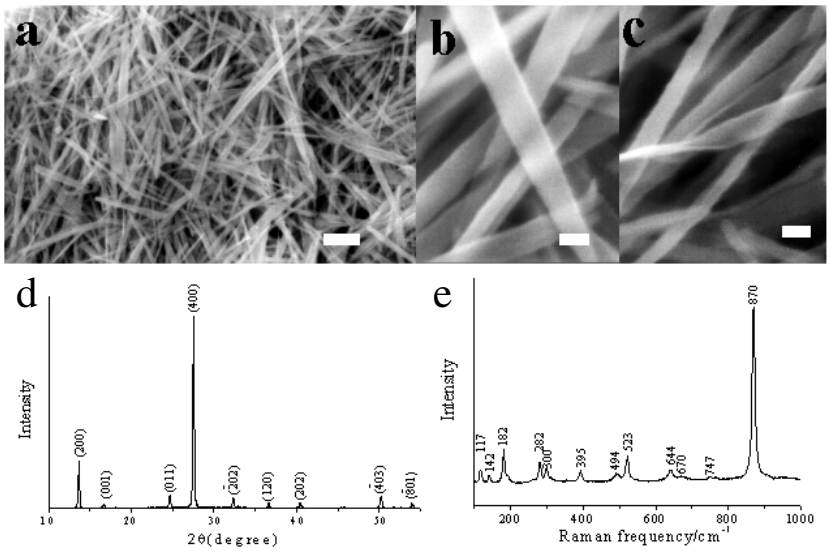

Figure 1. SEM images (a)–(c), XRD pattern (d) and Raman spectrum (e) of monoclinic raspite $PbWO_4$ nanobelts obtained in the presence of DexS-40. $[PbWO_4] = 5$ mM, [DexS-40] $= 1$ g l^{-1}. Scale bar: (a) 1 μm; (b), (c) 100 nm.

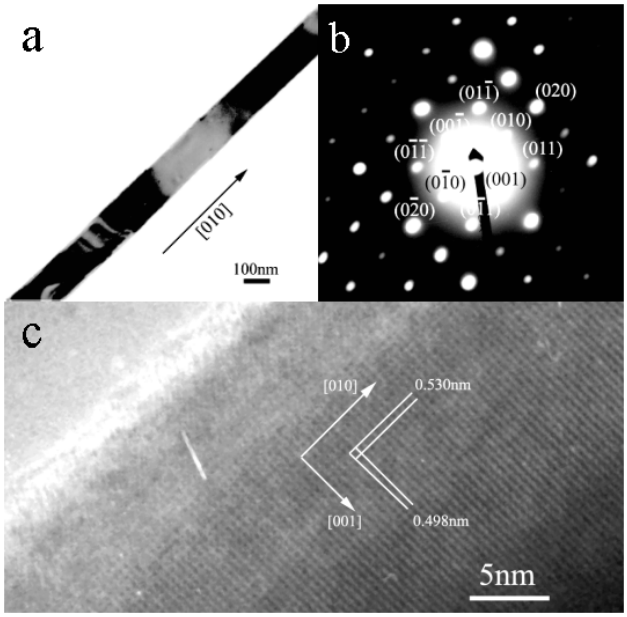

Figure 2. TEM image (a), ED pattern (b) and HRTEM image (c) of a monoclinic raspite $PbWO_4$ nanobelt. $[PbWO_4] = 5$ mM, [DexS-40] $= 1$ g l^{-1}.

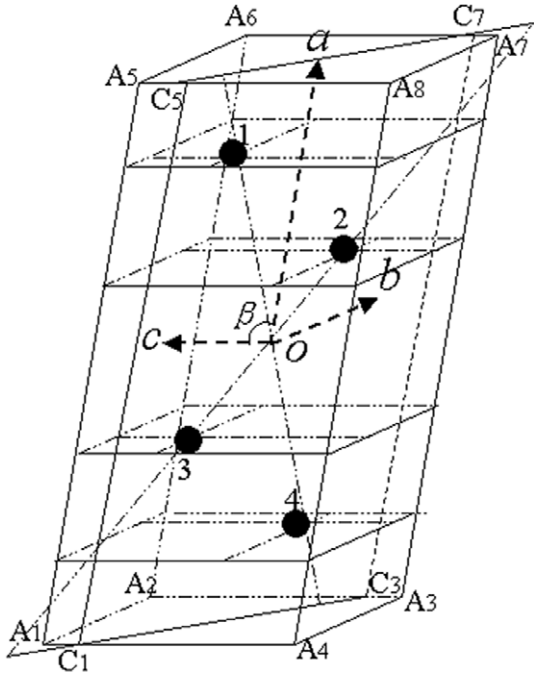

Figure 3. Illustration of Pb^{2+} coordinates in the unit cell of monoclinic raspite $PbWO_4$. Black atoms of Pb^{2+} were numbered.

reveals that the $PbWO_4$ nanoribbon is a single crystal with the top face bounded by the {100} planes. Furthermore, taking the TEM image of the single ribbon and its ED pattern (figures 2(a) and (b)) together, it leads to a conclusion that the growth direction of the nanoribbon is along the [010] direction. The nanoribbons were further characterized by HRTEM (figure 2(c)) and the fringe spacings of 0.498 and 0.530 nm agree well with the d-spaces of the (010) and (001) planes, indicating that the nanoribbon grows along the [010] direction with the top face of {100} planes, which is consistent with the indexing from the ED pattern.

For the $PbWO_4$ crystals with the monoclinic structure, the corresponding unit cell parameters of a, b and c are 13.52, 4.98 and 5.60 Å, respectively. As shown in figure 3, there are four Pb^{2+} ions numbered from 1 to 4 located in a unit cell, whose coordinates are (0.3504, −0.306, 0.1667), (0.1496, 0.1941, −0.1667), (−0.1496, −0.1941, 0.1667) and (−0.3504, 0.306, −0.1667), respectively. Theoretically, the face $C_1C_3C_7C_5$ that contains all four Pb^{2+} ions possesses the highest density of Pb^{2+} ions, though this face is unusual. According to the analysis and calculation, the density of Pb^{2+} ions in this face

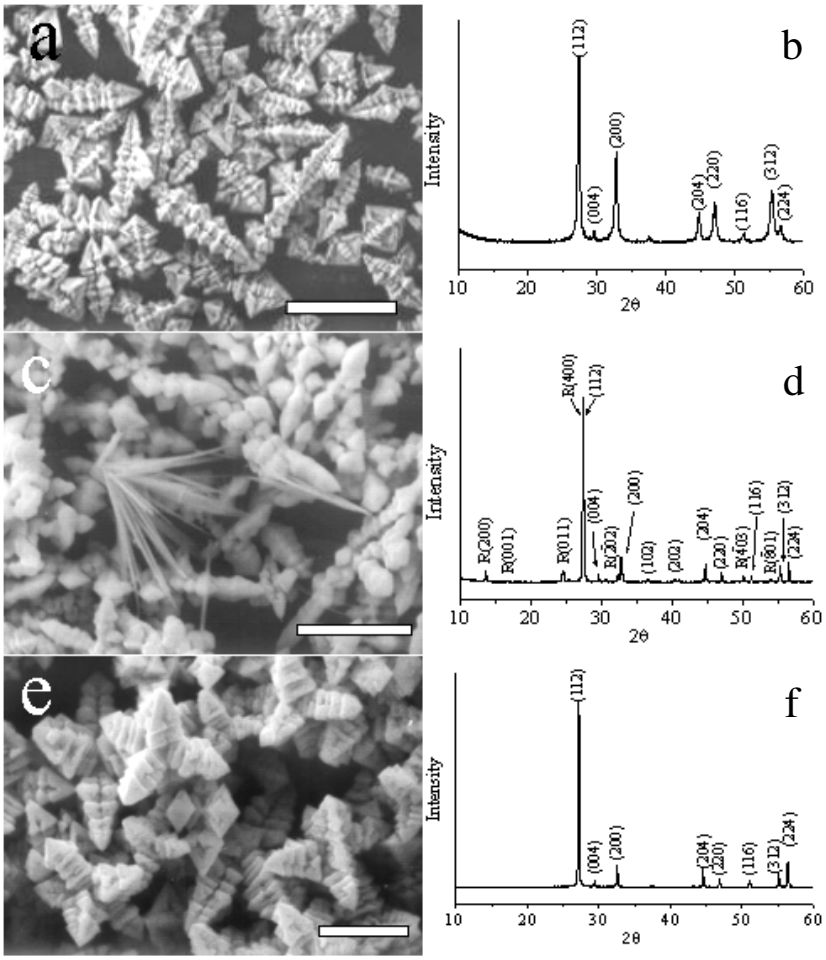

Figure 4. SEM images ((a), (c), (e)) and XRD patterns ((b), (d), (f)) of $PbWO_4$ crystals formed at various DexS-40 concentrations. The XRD patterns are indexed according to stolzite except for the index marked with 'R' denoting reflections from raspite. [$PbWO_4$] = 5 mM; [DexS-40]: (a), (b) 0 g l^{-1}; (c), (d) 0.5 g l^{-1}; (e), (f) 5 g l^{-1}. Scale bar: (a) 10 μm; (c) 5 μm; (e) 2 μm.

is about 0.045 $Å^{-2}$ and the face with a lower Pb^{2+} density is the (100) plane: $1/(4.98\ Å \times 5.60\ Å) = 0.036\ Å^{-2}$, which is the second largest density. In other words, the top faces of {100} of $PbWO_4$ nanoribbons are the planes where Pb^{2+} ions possess the highest packing density, except the unstable face of $C_1C_3C_7C_5$, suggesting that its Pb^{2+} density is higher than the other two possible exposure surfaces of the {010} and {001} planes. For example, the density of Pb^{2+} ions on the (010) and (001) faces is 0.028 $Å^{-2}$ $(2/(13.52\ Å \times 5.60\ Å \sin 107.7°))$ and 0.030 $Å^{-2}$ $(2/(13.52\ Å \times 4.98\ Å))$. So it is reasonable to conclude that the presence of DexS-40 with negatively charged SO_4^{2-} groups is a key factor for the formation of the nanobelts with the top face bound by the Pb^{2+}-enriched (100) planes, rather than the {010} and {001} planes, because this is stable in energy on account of the strong interaction between SO_4^{2-} groups and Pb^{2+} ions.

3.2. Effect of DexS-40 concentration

It was found that the concentration of DexS-40 greatly affects the morphology and crystal phase of $PbWO_4$ crystals. As shown in figure 4(a), pagoda-like $PbWO_4$ crystals with a size about 10 μm were formed in the absence of DexS-40, and the corresponding XRD pattern (figure 4(b)) indicates that the product is pure stolzite $PbWO_4$ crystals with the tetragonal structure (JCPDS card no. 85-1857). Furthermore, based on the experiments conducted without additives, we found that reactant concentrations had little effect on the morphology and structure of the crystals, confirming that the formation of tetragonal $PbWO_4$ is a predominant process in aqueous solution without additives. When 0.5 g l^{-1} DexS-40 was added to the solution, a small amount of $PbWO_4$ nanoribbons were formed in addition to the pagoda-like crystals, which may indicate that the presence of small amounts of the DexS-40 molecule is favourable for the formation of nanoribbon with the monoclinic raspite structure (figures 4(c) and (d)). As shown in figure 1, pure monoclinic $PbWO_4$ crystals were produced at a DexS-40 concentration of 1 g l^{-1}, which is slightly higher than 0.5 g l^{-1}. It is interesting to note that the monoclinic raspite $PbWO_4$ crystals transformed into tetragonal stolzite crystals with typical tetra-bipyramid morphologies when the DexS-40 concentration was further increased to 5 g l^{-1} (figure 4(e)). The corresponding XRD pattern shown in figure 4(f) confirms that the tetra-bipyramid products were pure stolzite $PbWO_4$ crystals with the tetragonal

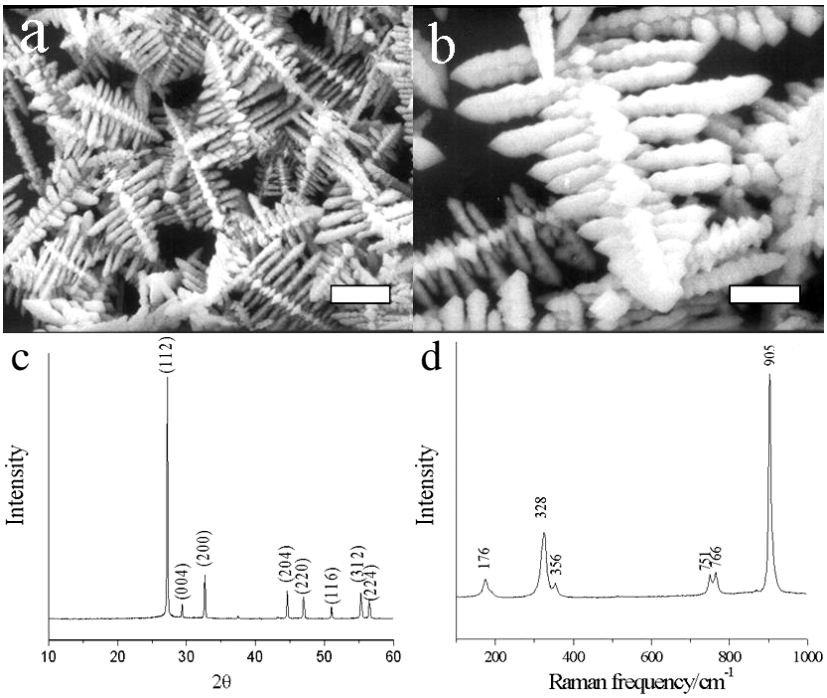

Figure 5. SEM images ((a), (b)), XRD pattern (c) and Raman spectrum (d) of stolzite $PbWO_4$ crystals formed in the presence of AM-Dex-5. $[PbWO_4] = 10$ mM; [AM-Dex-5] $= 10$ g l^{-1}. Scale bar: (a) 2 μm; (b) 1 μm.

structure. This kind of polymer-directed conversion of $PbWO_4$ from tetragonal to monoclinic and then to tetragonal again is unusual. Based on the experiments, it may be reasonably proposed that the formation of nanoribbons with the Pb^{2+}-enriched top faces would be favoured due to the specific interaction between SO_4^{2-} and Pb^{2+} at an appropriate DexS-40 concentration, which could considerably lower the surface energy. Assuming that there exists an optimal ratio of SO_4^{2-}/Pb^{2+} where the SO_4^{2-} groups from DexS-40 could interact with the Pb^{2+} ions from $PbWO_4$ crystals in the most effective way, there would be an optimal DexS-40 concentration for the formation of pure raspite $PbWO_4$ nanoribbons of the monoclinic structure. If the DexS-40 concentration exceeds the optimal concentration, the excess DexS-40 molecules would not enhance the interactions of Pb^{2+} and SO_4^{2-} to lower the overall energy but significantly inhibit the crystal growth, which is favourable for the generation of the thermodynamically stable tetragonal $PbWO_4$ crystals. However, further study is required to fully elucidate the mechanism at the molecular scale. In general, the crystallization process of crystals is very complex, and involves many factors related to thermodynamics and kinetics. For the raspite $PbWO_4$ nanoribbons, the interaction between SO_4^{2-} groups in DexS-40 and Pb^{2+} was considered to be a main factor determining the preferential formation of specific planes with higher density of Pb^{2+}. Nevertheless, it is still difficult to directly apply this mechanism to explain the morphological evolution of the stolzite $PbWO_4$ crystals shown in figure 4, i.e., from pagoda-like to tetra-pyramidal shapes; the inherent crystallization habit of tetragonal $PbWO_4$ could play an important role in this case.

3.3. Effect of differently charged dextrans

For investigating the influence of the electrical properties and functional groups of the dextrans on the crystallization of $PbWO_4$ crystals, the cationic dextran AM-Dex-5 and the nonionic dextran Dex-40 were introduced into the synthetic system. As shown in figure 5(a), novel penniform $PbWO_4$ crystals were formed in the presence of the cationic dextran AM-dex-5. From the enlarged SEM image of individual crystals, it can be observed that the axis of the feather crystal is about 4–7 μm in length with side rods (up to 2 μm in length) growing in parallel on both sides. The XRD pattern of the product reveals that the penniform $PbWO_4$ crystals are tetragonal-structured crystals (figure 5(c)). The corresponding Raman spectrum (figure 5(d)) displays sharp peaks at 176, 328, 356, 751, 766 and 905 cm^{-1}, characteristic of stolzite, in good agreement with the XRD result. The formation of such penniform products with the tetragonal structure is interesting, but not rare. For instance, penniform $BaXO_4$ (X = W, Cr, Mo) crystals have been synthesized in cationic reverse micellar systems under mild conditions [17, 18] and fishbone-like $PbWO_4$ crystals were prepared by the polymer-directed process [30]. Moreover, wheat-ear-like $PbWO_4$ crystals were produced in the presence of the nonionic dextran Dex-40 (figure 6). The related XRD pattern also indicates the tetragonal structure of the product. In addition, the influence of both AM-Dex-5 and Dex-40 concentrations on the $PbWO_4$ crystals was investigated and it was found that the concentration of the cationic and nonionic dextrans did not show remarkable effects on the morphology of the obtained stolzite $PbWO_4$ crystals. To summarize, feather-like and wheat-ear-like stolzite $PbWO_4$ crystals were produced

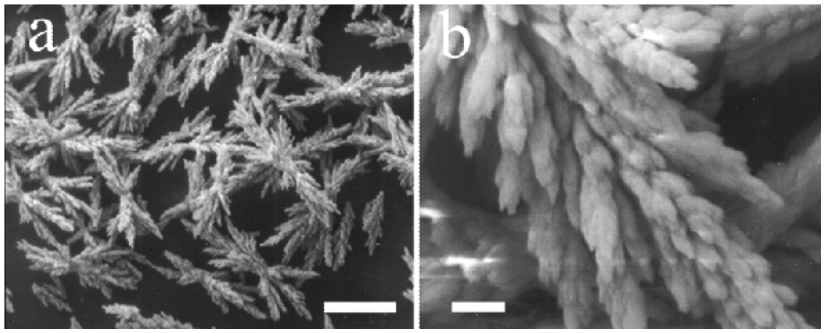

Figure 6. SEM images of stolzite $PbWO_4$ crystals formed in the presence of Dex-40. [$PbWO_4$] = 5 mM. [Dex-40]:1 g l^{-1}. Scale bar: (a) 10 μm; (b) 1 μm.

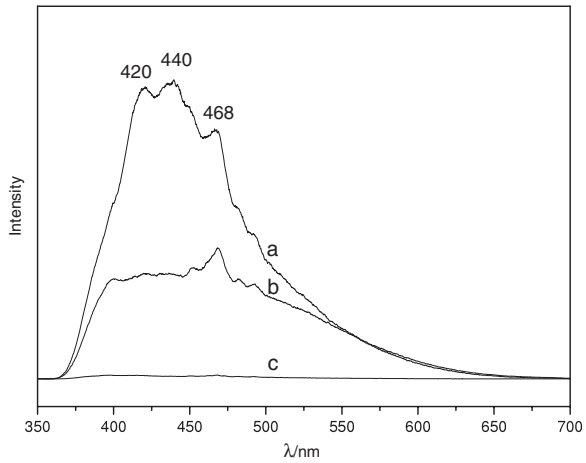

Figure 7. Photoluminescence spectra of $PbWO_4$ crystals with different morphologies and structures. (a) Stolzite feathers, (b) stolzite tetra-bipyramids, (c) raspite nanobelts.

in the presence of cationic AM-Dex-5 and nonionic Dex-40, respectively; on the other hand, in the presence of anionic DexS-40, raspite $PbWO_4$ nanobelts were obtained at suitable dextran concentrations whereas stolzite $PbWO_4$ crystals with pagoda-like and tetra-pyramidal shapes were obtained at lower and higher dextran concentrations, respectively. In brief, only stolzite-structured $PbWO_4$ crystals were formed in the presence of cationic or nonionic dextrans although the morphologies of products were modulated significantly, demonstrating that the anionic dextran can effectively control both the morphology and structure of $PbWO_4$ crystals due to the strong, specific interactions of the SO_4^{2-} groups and the Pb^{2+} ions.

3.4. Photoluminescence characteristics of $PbWO_4$ crystals

Figure 7 shows the room-temperature photoluminescence (PL) spectra of the as-synthesized $PbWO_4$ crystals with different morphologies and structures using an excitation line of 350 nm. The PL spectrum of the stolzite $PbWO_4$ feathers obtained in the presence of AM-Dex-5 displays intensive blue emissions with three main emission bands located at 420, 440 and 468 nm (figure 7(a)). In contrast, the stolzite tetra-bipyramids obtained in the presence of 5 g l^{-1} DexS-40 show relatively weak and broad luminescence in the range 370–650 nm with a notable peak around 468 nm (figure 7(b)). It has been well known that there appear to be two emission bands in stolzite $PbWO_4$ crystals of the tetragonal scheelite structure, i.e. the intrinsic 'blue' band around 440 nm and the 'green' band in the range 500–540 nm [20]. The blue band is admittedly originated from tetragonal WO_4^{2-} groups [48] while the origin of the green band still remains controversial [49, 50]. In the current situation, both stolzite products did not show clear green emission and the location and relative intensity of the blue emissions seemed to be closely related to the crystal morphology. This result is not very surprising considering that the luminescence properties of $PbWO_4$ crystals are very sensitive to their synthesis conditions and structural defects [30, 38, 39]. On the other hand, the PL spectrum of the monoclinic raspite $PbWO_4$ nanobelts obtained in the presence of 1 g l^{-1} DexS-40 exhibits only negligible luminescence in the visible-light region (figure 7(c)). It is noted that a green emission around 550 nm (2.25 eV) has been observed at 6 K for the natural raspite crystals [20]. The absence of obvious emission at 550 nm for the synthesized raspite $PbWO_4$ nanobelts could be ascribed to the structural defects or the lowered PL intensity at room temperature. Moreover, the structural order–disorder in the raspite crystal lattice could play a key role in the PL properties, considering that the generation of the intense visible PL band stolzite $PbWO_4$ crystals is related to simultaneous structural order and disorder in the crystal lattice [50]. In short, the luminescent properties of $PbWO_4$ crystals are closely related to the morphology, crystal structure as well as structural defects and detailed investigation is needed to unambiguously interpret the luminescent properties of $PbWO_4$ crystals. Obviously, the realization of the synthesis of raspite crystals in the laboratory provides a good opportunity for such fundamental studies.

4. Conclusions

A variety of $PbWO_4$ crystals with modulated morphologies and polymorphs, such as monoclinic raspite $PbWO_4$ nanobelts and tetragonal stolzite $PbWO_4$ crystals with penniform and wheat-ear-like morphologies, were successfully synthesized by a facile solution route in the presence of differently charged dextrans. Novel monoclinic raspite $PbWO_4$ nanobelts were produced under the direction of the anionic dextran sulfate,

probably due to the specific interactions between SO_4^{2-} groups from anionic dextran molecules and Pb^{2+} ions from $PbWO_4$ crystals. This is the first laboratory synthesis of raspite $PbWO_4$ crystals with the monoclinic structure, which may be beneficial for fundamental studies and potential applications of $PbWO_4$ crystals. In addition, the room-temperature photoluminescence properties of the obtained $PbWO_4$ crystals with different morphologies and crystal structures were characterized; it was found that the feather-like stolzite $PbWO_4$ crystals displayed intensive blue emissions whereas the raspite $PbWO_4$ nanobelts just showed negligible emission in the visible-light region. The obtained results demonstrate that dextrans are effective modifiers for the $PbWO_4$ crystallization and such an approach may be potentially extended to the morphology- and structure-controlled synthesis of inorganic functional materials other than $PbWO_4$ crystals.

Acknowledgments

This work was supported by NSFC and MOST (2007CB936201).

References

[1] Burda C, Chen X, Narayanan R and El-Sayed M A 2005 *Chem. Rev.* **105** 1025
[2] Yin Y and Alivisatos A P 2005 *Nature* **437** 664
[3] Jun Y, Choi J and Cheon J 2006 *Angew. Chem. Int. Edn* **45** 3414
[4] Wiley B, Sun Y, Chen J, Cang H, Li Z-Y, Li X and Xia Y 2005 *MRS Bull.* **30** 356
[5] Cölfen H and Mann S 2003 *Angew. Chem. Int. Edn* **42** 2350
[6] Duan X F, Huang Y, Cui Y, Wang J F and Lieber C M 2001 *Nature* **409** 66
[7] Huang M, Mao S, Feick H, Yan H, Wu Y, Kind H, Weber E, Russo R and Yang P 2001 *Science* **292** 1897
[8] Pan Z W, Dai Z R and Wang Z L 2001 *Science* **291** 1947
[9] Wang X, Song J, Liu J and Wang Z L 2007 *Science* **316** 102
[10] Mao C, Wu X, Pan H, Zhu J and Chen H 2005 *Nanotechnology* **16** 2892
[11] Zhang H, Zuo M, Tan S, Li G and Zhang S 2006 *Nanotechnology* **17** 2931
[12] Yu S, Antonietti M, Colfen H and Giersig M 2002 *Angew. Chem. Int. Edn* **41** 2356
[13] Liao H, Wang Y, Liu X, Li Y and Qian Y 2000 *Chem. Mater.* **12** 2819
[14] Xie B, Wu Y, Jiang Y, Li F, Wu J, Yuan S, Yu W and Qian Y 2002 *J. Cryst. Growth* **235** 283
[15] Chen S, Zhou J, Chen X, Li J, Li L, Hong J, Xue Z and You X 2003 *Chem. Phys. Lett.* **375** 185
[16] Lei S, Tang K, Fang Z, Huang Y and Zheng H 2005 *Nanotechnology* **16** 2407
[17] Shi H, Qi L, Ma J and Cheng H 2003 *J. Am. Chem. Soc.* **125** 3450
[18] Shi H, Qi L, Ma J and Wu N 2005 *Adv. Funct. Mater.* **15** 442
[19] Kwan S, Kim F, Akana J and Yang P 2001 *Chem. Commun.* 447
[20] Itoh M and Fujita M 2000 *Phys. Rev.* B **62** 12825
[21] Gratta G, Newman H and Zhu R 1994 *Annu. Rev. Nucl. Part. Sci.* **44** 453
[22] Anderson S 1993 *Nucl. Instrum. Methods Phys. Res.* A **332** 373
[23] Nikl M, Nitsch K, Hybler J, Chval J and Reiche P 1996 *Phys. Status Solidi* **196** K7
[24] Liu T, Zhang Q and Zhuang S 2007 *Opt. Mater.* **29** 1044
[25] Bastians S, Crump G, Griffith W and Withnall R 2004 *J. Raman Spectrosc.* **35** 726
[26] Nitsch K, Nikl M, Ganschow S, Reiche P and Uecker R 1996 *J. Cryst. Growth* **165** 163
[27] Tanji K, Ishii M, Usuki Y, Kobayashi M, Hara K and Takano H 1999 *J. Cryst. Growth* **204** 505
[28] Hu X and Zhu Y 2004 *Langmuir* **20** 1521
[29] Chen D, Shen G, Tang K and Liang Z 2004 *J. Phys. Chem.* B **108** 11280
[30] Yu J, Zhao X, Liu S, Li M, Mann S and Ng D 2007 *Appl. Phys.* A **87** 113
[31] Geng J, Zhu J, Lu D and Chen H 2006 *Inorg. Chem.* **45** 8403
[32] Zhao G, Lu M, Gu F, Yu D and Yuan D 2005 *J. Cryst. Growth* **276** 577
[33] Liu B, Yu S, Li L and Zhang Q 2004 *Angew. Chem. Int. Edn* **43** 4745
[34] Zhang Q, Yao W, Chen X, Zhu Li, Fu Y, Zhang G, Sheng L and Yu S 2007 *Cryst. Growth Des.* **7** 1423
[35] Liu S, Yu J, Zhao X and Cheng B 2007 *J. Alloys Compounds* **433** 73
[36] Huo L and Chu Y 2006 *Mater. Lett.* **60** 2675
[37] He X and Cao M 2006 *Nanotechnology* **17** 3139
[38] Geng J, Zhu J and Chen H 2006 *Cryst. Growth Des.* **6** 321
[39] Geng J, Lu Y, Lu D and Zhu J 2006 *Nanotechnology* **17** 2614
[40] Kloprogge J, Weier M, Duong L and Frost R 2004 *Mater. Chem. Phys.* **88** 438
[41] Qi L, Cölfen H and Antonietti M 2000 *Angew. Chem. Int. Edn* **39** 604
[42] Yu S, Antonietti M, Cölfen H and Hartmann J 2003 *Nano Lett.* **3** 379
[43] Xu A-W, Ma Y and Cölfen H 2007 *J. Mater. Chem.* **17** 415
[44] Aizawa H, Hu S, Bobb K, Balakrishnan K, Ince G, Gurevich I, Cowan M and Ghosh A 2004 *Science* **303** 197
[45] Aizenberg J, Lambert G, Weiner S and Addaddi L 2002 *J. Am. Chem. Soc.* **124** 32
[46] Yang J, Qi L, Zhang D, Ma J and Cheng H 2004 *Cryst. Growth Des.* **4** 1371
[47] Yang J, Qi L, Lu C, Ma J and Cheng H 2005 *Angew. Chem. Int. Edn* **44** 598
[48] Van Loo W 1975 *Phys. Status Solidi* a **27** 565
[49] Babin V, Bohacek P, Krasnikov A, Nikl M, Stolovits A and Zazubovich S 2007 *J. Lumin.* **124** 113
[50] Anicete-Santos M *et al* 2007 *Phys. Rev.* B **75** 165105